The influence of substitutional disorder on the structural phase transitions in $Rb_{1-x}K_xCaF_3$ (x<or=0.2) mixed perovskite crystals

1994 J. Phys.: Condens. Matter 6 2189

(http://iopscience.iop.org/0953-8984/6/11/008)

J. Phys.: Condens. Matter 6 (1994) 2189–2206. Printed in the UK

The influence of substitutional disorder on the structural phase transitions in $Rb_{1-x}K_xCaF_3$ ($x \leqslant 0.2$) mixed perovskite crystals

A M Debaud-Minorel and J Y Buzaré

Equipe de Physique de l'Etat Condensé, Unité de Recherche Associée au CNRS No 807, Université du Maine, Avenue O Messiaen, 72017 Le Mans Cédex, France

Received 21 October 1993, in final form 29 November 1993

Abstract. The influence of ionic substitution on the phase transitions in mixed $Rb_{1-x}K_xCaF_3$ fluoroperovskite crystals ($x \leqslant 0.2$) is studied by EPR of the Gd^{3+}–O^{2-} pair substituted for a Ca^{2+}–F^- bond as a local probe. The behaviour of the EPR spectra versus temperature reveals the existence of two successive first-order phase transitions associated with CaF_6 octahedron rotation. Computer reconstructions of the EPR spectra allow us to conclude that, in the low-temperature phase, the CaF_6 octahedra are rotated by three equal angles around the fourfold cubic axes. Then, we were able to determine the variations of the total rotational angle ϕ defined by $\phi^2 = \phi^2_{[100]} + \phi^2_{[010]} + \phi^2_{[001]} = 3\phi^2_{[001]}$. It is observed to increase continuously for $x = 0.05$ whereas a discontinuity towards larger values occurs in the $x = 0.2$ compound. The phase diagram drawn from the EPR measurements shows that the transition temperatures are enhanced with increasing x and the temperature range over which the tetragonal phase exists tends to become smaller. These results lead to the conclusion that the occurrence of the phase transitions is related to the compactness of the unit cell and that the substitution enhances the instabilities at the M and R points of the Brillouin zone.

1. Introduction

Perovskite crystals AMF_3 have attracted a great deal of interest in recent years because of their simple structure and their ability to undergo phase transitions associated with octahedron rotations. Nevertheless, they may exhibit quite different symmetries at room temperature and different sequences of phase transitions. Indeed, $RbCaF_3$ is cubic at room temperature and undergoes a weakly first-order structural phase transition (SPT) at 195 K induced by the mode condensation at the R point of the cubic Brillouin zone. This is followed at 50 K by a second SPT involving simultaneous mode condensations at the M and R points.

On the other hand, $KCaF_3$ is cubic at high temperature ($T > 560$ K) and undergoes two successive SPTs leading the crystal into an orthorhombic phase. The former is caused by mode condensation at the M and R points simultaneously, the latter by condensation at the R point only. The R soft mode consists of alternate rotations of the CaF_6 octahedra around one of the three fourfold axes; the M point is connected to non-alternate rotations of the same octahedra.

These differences between the behaviour of the two compounds give evidence of the important role of the cation A in stabilizing this type of structure. One may expect that the substitution of Rb^+ by K^+ ions should change the interactions and modify the correlations between adjacent CaF_6 octahedra.

0953-8984/94/112189+18$19.50

The purpose of this paper is to present recent EPR results on the mixed crystal $Rb_{1-x}K_xCaF_3$ ($x \leqslant 0.2$). Preliminary results have been previously published in [1] and [2] where important references may be found. In the present work, attention is paid essentially to the second strongly first-order SPT observed in the mixed crystal for $x > 0$ and the analysis of the low-temperature phase. We report on the results from experiments performed in X and K bands and some experiments under uniaxial stresses in the K band. We emphasize the influence of the concentration of the substitutional ion on the evolution of the order parameter versus temperature. Some conclusions about the relation between the phase transitions and the compactness of the unit cell are tentatively drawn from a comparison between our measurements and some results achieved in other mixed perovskite crystals [3–5].

2. Experimental details

Single crystals of $Rb_{1-x}K_xCaF_3$ used in these experiments were doped with Gd_2O_3 and grown by the Bridgman–Stockbarger method with the technical assistance of G Niesseron. Gd^{3+}–O^{2-} pairs, substituted for Ca^{2+}–F^- bonds, are used as structural local probes. These probes do not disturb the lattice very much since the radii of the substituted ions fit with those of the Ca^{2+} and the F^- ions.

The EPR spectra were recorded either on a Bruker X-band spectrometer ($\nu = 9.5$ GHz) or on the K-band spectrometer ($\nu = 19.5$ GHz) built in IBM Zurich Research Laboratory by W Berlinger† and given to us by K A Müller recently.

Experiments under application of uniaxial stresses were achieved by using the K-band spectrometer only. The stress was applied with a stainless-steel hollow force transmitting tube. Technical details on the apparatus may be found in [6], [7] and [8].

3. Temperature dependence of the Gd^{3+}–O^{2-} pair EPR spectra in pure $RbCaF_3$

The Gd^{3+}–O^{2-} pair can be viewed as a particular bond of a molecular $[GdOF_5]^{4-}$ entity. The corresponding paramagnetic centre constitutes an $^8S_{7/2}$ ion submitted to an axial distortion directed along the pair axis [9]. It is quite similar to the Fe^{3+}–V_O pair previously used to investigate critical phenomena in $SrTiO_3$ [10].

In the cubic phase, the angular dependence of the EPR lines when $\boldsymbol{H}$ rotates in the (001) plane gives evidence for three types of paramagnetic centre related to the Gd^{3+}–O^{2-} pairs lying along the three [100], [010] and [001] fourfold axes [11]. The EPR spectra have been interpreted with a spin Hamiltonian reflecting the tetragonal symmetry of the centre with a large value of the quadrupolar crystal-field parameter b_2^0 (0.26 cm^{-1}) [9, 11]. For $\boldsymbol{H}\|[110]$, the lines owing to pairs along [100] and [010] coincide while the pairs along [001] whose axis is perpendicular to the magnetic field direction correspond to a single line. Such lines are shown in figure 1(*a*). From this position, a rotation of the crystal by 1° around the [001] axis induces a splitting of 36 G between the two components of the high-field line. This high sensitivity allows us to investigate the octahedron rotations induced by the phase transitions through rotation of the pair axis in the magnetic field [12].

The corresponding spectrum in the tetragonal phase is shown in figure 1(*b*). The low-field line related to [001] pairs remains unchanged in this phase while the lines related to

† Deceased.

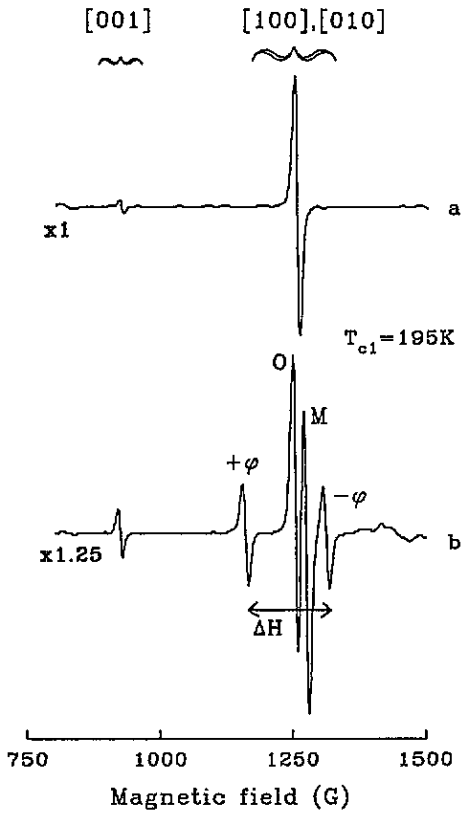

Figure 1. The temperature dependence of the A lines in $RbCaF_3$ about the first SPT in the X band (H_{rf}‖[001], H‖[110]): (*a*) $T = 300$ K; (*b*) $T = 165$ K.

the pairs along the other two fourfold axes split into four components referred to as $+\phi$, $-\phi$, O, M. Figure 2 specifies the different centres related to these lines. The $\pm\phi$ lines may be attributed to pairs in [001] domains: the pair axes lie at $45° \pm \phi$ away from the magnetic field; the splitting ΔH has been previously shown to be proportional to ϕ, which is the order parameter of the transition, and we may write $\Delta H = B\phi$ with $B = 36$ G/d° [12]. The M line is due to [100] (respectively [010]) pairs in [010] (respectively [100]) tetragonal domains. The O line arises from pairs lying along the domain axis in [100] or [010] domains.

From the splitting of the $\pm\phi$ lines in the tetragonal phase, we have deduced the values of the order parameter versus temperature down to 4.2 K where, surprisingly, the spectra are still compatible with a tetragonal phase where $\phi = 7.9°$. Indeed, in powdered samples, a second SPT has been observed at $T_{c2} = 50$ K [13, 14]. This behaviour may be attributed to internal strains in the crystal, which do not exist in powder. These strains strongly affect the transition temperature by keeping the crystal in the tetragonal phase.

More generally, an octahedron rotation has to be described with two parameters: the rotational axis direction and the rotational angle. For small angles and any direction, we may write

$$\vec{\phi} = \vec{\phi}_{[100]} + \vec{\phi}_{[010]} + \vec{\phi}_{[001]}.$$

From the line splittings observed in the tetragonal phase, it may be inferred that, when the magnetic field is along a twofold axis, the line splitting induced by any octahedral

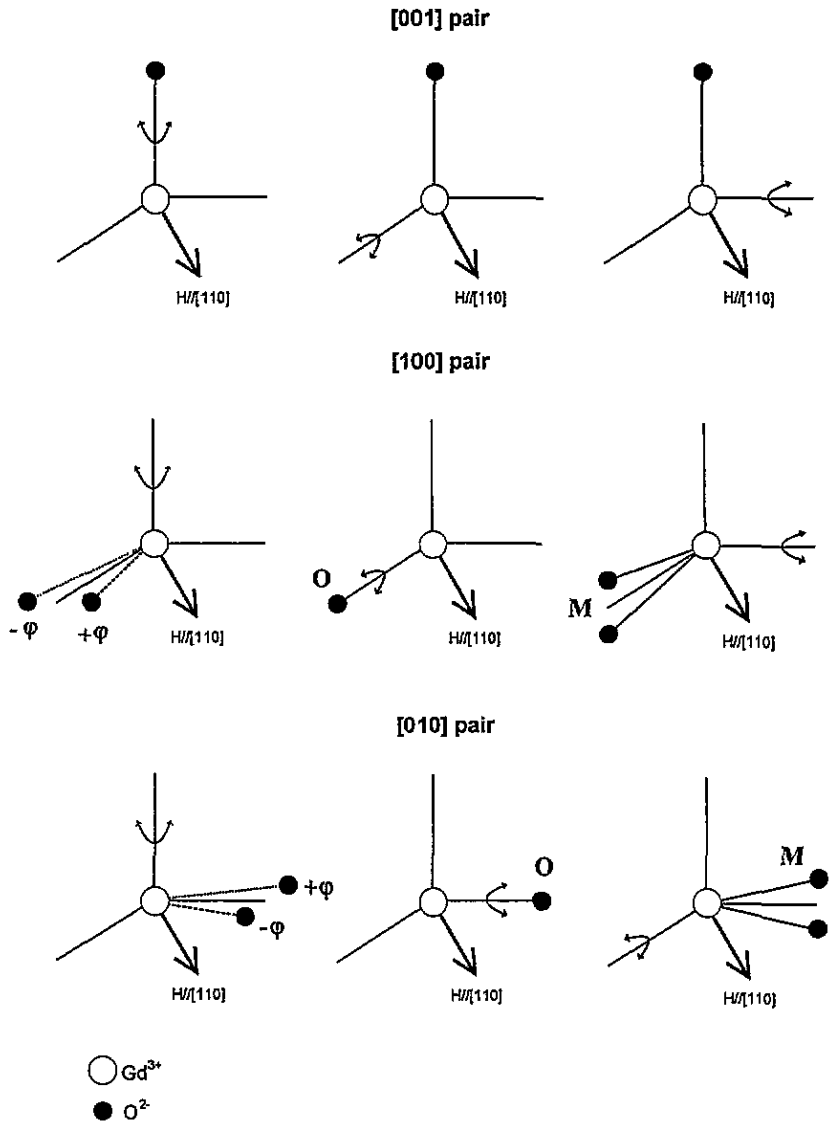

Figure 2. The different Gd^{3+}–O^{2-} pairs in the tetragonal phase.

rotational vector $\vec{\phi}$ is proportional to the vector component, that lies along the fourfold cubic axis perpendicular to the magnetic field.

Then, whatever the $\vec{\phi}$ direction is, ΔH deduced from the $\pm\phi$ line splitting is proportional to $\phi_{[001]}$ which is the $\vec{\phi}$ component perpendicular to the magnetic field axis ($\boldsymbol{H}\|[110]$ in our experiments) [16, 17].

4. Temperature dependence of the EPR spectra in the mixed perovskite

In the mixed crystals, the resolution of the spectra lowers when x increases, so measurements were achieved for $Rb_{1-x}K_xCaF_3$ crystals with low values of x (0.05, 0.2).

4.1. $Rb_{0.95}K_{0.05}CaF_3$

Typical spectra obtained at X band and K band ($H \| [110]$) in the different phases are given in figures 3 and 4 respectively. As can be seen, the essential features of the Gd^{3+}–O^{2-} pair spectrum in pure $RbCaF_3$ remain. The spectra corresponding to the cubic phase are shown in figures 3(*a*) and 4(*a*): the low-field line with weaker intensity is related to pairs along [001], the other line to pairs along [100] and [010]. Nevertheless, the lines are broadened and flanked by satellites, which may be attributed to pairs surrounded by n K^+ and $(8-n)$ Rb^+ as next-nearest neighbours ($n = 1, 2, \ldots, 8$). Indeed, the substitution of K^+ for Rb^+ ions in the $RbCaF_3$ cell lowers the local symmetry of the crystal field at the Gd^{3+} site. The corresponding spin Hamiltonian parameters have been previously determined and it was concluded that the K^+ and Rb^+ ions are distributed at random [1]. The intensity of these extra lines is more important for the crystal with $x = 20\%$.

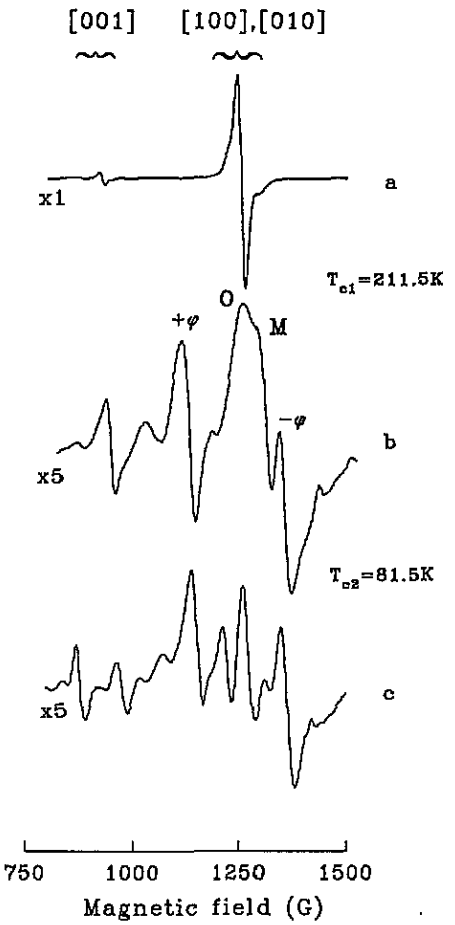

Figure 3. The temperature dependence of the A lines in $Rb_{0.95}K_{0.05}CaF_3$ in the X band ($H_{rf} \| [001]$, $H \| [110]$): (*a*) $T = 300$ K; (*b*) $T = 165$ K; (*c*) $T = 50$ K.

In opposition to the pure compound $RbCaF_3$ where only one SPT has been observed, the evolution of the spectra in $Rb_{0.95}K_{0.05}CaF_3$ evidences two successive SPTs for the two

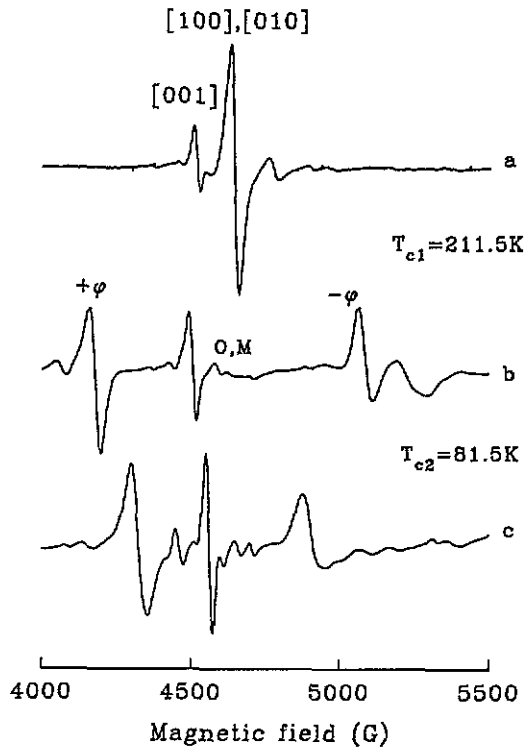

Figure 4. The temperature dependence of the B and C lines in the K band (H_{rf}‖[001], H‖[110]): (*a*) $T = 300$ K: (*b*) $T = 124$ K; (*c*) $T = 79$ K.

values of x (figures 3(*b*,*c*) and 4(*b*,*c*)). The existence of this second transition shows that the disorder induced by the substitution of Rb^+ by K^+ may relax the internal strains. The two transition temperatures deduced from our measurements with the K-band spectrometer are given in table 1.

Table 1. Transition temperatures in the mixed perovskite crystal $Rb_{1-x}K_xCaF_3$. The measurements were achieved in the K band.

x	T_{c1} (K)	T_{c2} (K)
0	195	not observed
0.05	*211.5 ± 0.5*	*81.5 ± 0.5*
0.2	246.5 ± 1.0	162.4 ± 1.0

4.1.1. The tetragonal phase. In figures 3(*b*) and 4(*b*), despite larger linewidths, the spectra may be related to a tetragonal phase with the characteristic $\pm\phi$, O and M lines related to pairs along [100] and [010] cubic axes as previously described in the pure compound. The line connected with Gd^{3+}–O^{2-} pairs along [001] is not affected by the transition at $T_{c1} = 211.5$ K in $Rb_{0.95}K_{0.05}CaF_3$. In the K band, the O and M lines of relatively low intensity are nearly superimposed in this spectrum. This is in agreement with preponderant [001] domains. Furthermore, we obtain $\Delta H = B\phi$ with $B = 156$ G/d°. This large value results in the $\pm\phi$ lines lying on either side of the [001] component.

4.1.2. The low-temperature phase. Below $T_{c2} = 81.5$ K, the removal of the tetragonal symmetry modifies the spectra.

The K-band spectrum (figure 4(*c*)) may be easily understood: the line due to [001] pairs leads to the two inner lines. On the other hand, the splitting between the $\pm\phi$ tetragonal lines decreases abruptly at T_{c2} when the O and M lines split into two components superimposed on the $\pm\phi$ lines, as may be inferred from the enhancement of the intensity of these lines at T_{c2}.

The evolution of the $\pm\phi$ line splitting versus temperature leads to the following measurements:

$$\text{at } T_{c2}+\epsilon \qquad \phi_{[001]} = 6.9 \pm 0.1^\circ \qquad \phi = \phi_{[001]}$$

$$\text{at } T_{c2}-\epsilon \qquad \phi_{[001]} = 3.8 \pm 0.1^\circ.$$

Now, $3.8/6.9 \simeq 1/\sqrt{3} = \cos(54°44')$, therefore the rotational vector $\vec{\phi}$, which lies along a $\langle 100\rangle$ direction in the tetragonal phase with $\|\vec{\phi}\| = 6.9°$, would undergo an abrupt change of direction towards a $\langle 111\rangle$ axis without modification of $\|\vec{\phi}\|$ at T_{c2}.

In the X band, the analysis of the spectrum is not so straightforward (figure 3(*c*)). The line related to [001] pairs splits into two components; the lines due to [100] and [010] pairs give rise to five components at least. In order to fully understand such a spectrum, it was necessary to undertake computer simulations, which are presented in the following part of the paper.

The satellite lines do not seem to be affected by the two SPTs: neither the linewidth and the lineshape nor the intensity of these lines are modified by the two transitions.

4.2. $Rb_{0.8}K_{0.2}CaF_3$

The temperature dependence of typical spectra obtained in the K band for the compound with $x = 0.2$ is presented in figure 5. The main point is the enhancement of the transition temperatures connected with the substitution (see table 1).

Studying the behaviour of these spectra is now much more difficult because of an important linewidth and the existence of lines due to pairs surrounded by one or two K^+ ions as next-nearest neighbours, but, we can recognize firstly, the four lines characteristic of the tetragonal phase ($\pm\phi$, O and M) and secondly, the line related to the [001] pairs in figure 5(*b*). Finally in the low-temperature phase (figure 5(*c*)), a similar behaviour to that in $Rb_{0.95}K_{0.05}CaF_3$ is observed. However, the linewidths prevent us from drawing conclusions about the transition effects on the satellites. We can add that this transition remains first order.

4.3. Experiments under uniaxial stresses

In order to obtain additional information about the low-temperature phase, we carried out some experiments under uniaxial stresses with the K-band spectrometer on $Rb_{0.95}K_{0.05}CaF_3$ only. Some experiments were achieved in the pure compound in the recent past with the same apparatus, which led to important conclusions on the influence of external stresses on the phase transitions in perovskite [15–18]. The geometry of the apparatus allows application of the stress perpendicular to the external magnetic field H. Compressional stresses were applied along $\langle 100\rangle$ or $\langle 110\rangle$ directions.

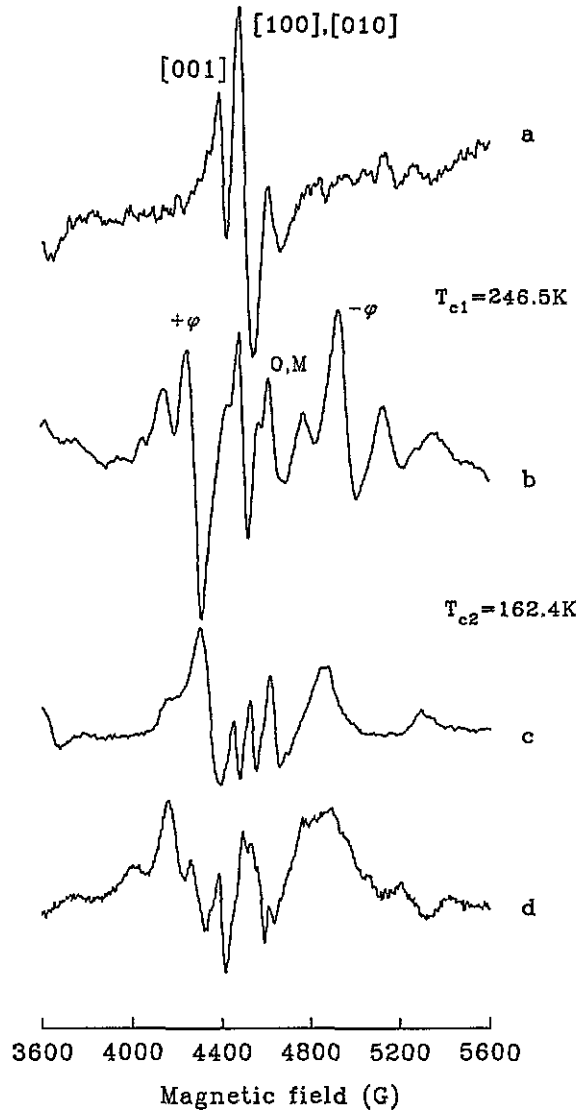

Figure 5. The temperature dependence of the B and C lines in $Rb_{0.8}K_{0.2}CaF_3$ in the K band (H_{rf}‖[001], $H_{\parallel}$[110]): (*a*) $T = 300$ K; (*b*) $T = 200$ K; (*c*) $T = 145$ K; (*d*) $T = 86$ K.

4.3.1. σ‖[001]. Under small [001] stress below T_{c1}, only [100] and [010] domains are observed, which leads to the disappearance of the $\pm\phi$ lines on the spectra. In the tetragonal phase, a typical spectrum consists of the two O and M lines and the line related to [001] pairs. This spectrum looks like the spectrum in the cubic phase, which prevents us from an accurate measurement of T_{c1}. No definite conclusion about an alteration of T_{c1} can be drawn from this experiment, but one interesting point is that the first SPT remains first order in the accessible stress range.

In the low-temperature phase, neither the spectra nor T_{c2} is affected by the stress, whatever the intensity of the stress is.

4.3.2. $\sigma \| [110]$. For a small applied [110] stress, only a [001] domain was observed, which leads to the existence of $\pm\phi$ lines and those related to the [001] pairs in the spectra of the tetragonal phase. We have measured T_{c1} and T_{c2} for two values of the stress. The scheme deduced from our measurements is presented in figure 6. It leads to $dT_{c1}/d\sigma = 14$ K kbar^{-1}. In pure $RbCaF_3$, $dT_{c1}/d\sigma = 7.6$ K kbar^{-1} [18]. The coexistence domain of the cubic and tetragonal phases increases with the intensity of the stress. At T_{c1}, from the splitting of the $\pm\phi$ lines, we deduced $\phi = 1.5°$ whatever the applied stress when one measured $\phi = 1.85°$ in pure $RbCaF_3$ [18]. The splitting does not seem to be affected by the stress in the two compounds. We have also verified that the transition remains first order for this type of stress. The external stress does not affect the EPR spectra in the low-temperature phase below T_{c2}.

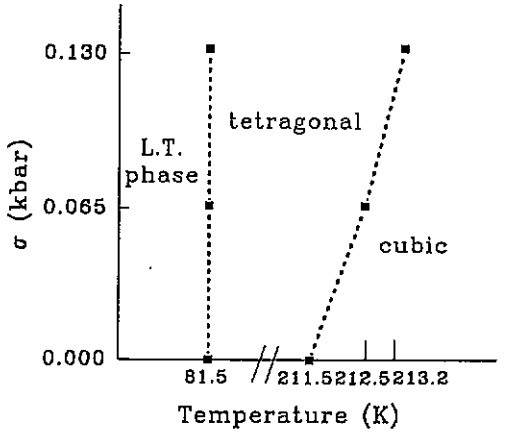

Figure 6. The phase diagram $\sigma(T)$ in $Rb_{0.95}K_{0.05}CaF_3$.

We have to mention that the mixed crystal is particularly sensitive to low temperature and external stress. Cleavage lines can be observed in the crystal even for a weak intensity of the stress. No other conclusions can be extracted from these experiments because of the brittleness of the mixed compound, which could not support higher stresses. This phenomenon may be easily attributed to the substitutional ions in the crystal.

5. Reconstructions of spectra in the low-temperature phase

5.1. Basic assumptions

As has been indicated above, some essential features of the spectra in the low-temperature phase could be interpreted by assuming ⟨111⟩ rotated octahedra.

This assumption could also explain

(i) the observed splitting of the lines into two components related to the [001] pairs when the magnetic field lies along the [110] axis and

(ii) the observed splitting of the lines into three components when the magnetic field lies along one [111] axis direction.

Finally, the ionic radius of the K^+ ion is smaller than the Rb^+ one. The substitution takes place in the ⟨111⟩ directions, which could favour the octahedron rotations around these axes.

Even if this assumption seems to be correct in the K band, it is less obvious for most spectra in the X band. In fact, the multiplicity of components of some lines may remain at first sight unexplained in this description. Then, in the low-temperature phase, the spectra will be simulated by assuming rotated octahedra around the three fourfold cubic axes by equal angles.

5.2. Computer simulation of the EPR spectra

From our point of view, a multicomponent spectrum as in figure 3(*c*), which cannot be easily explained by rigid octahedron rotations, evidences alterations of the values of the spin Hamiltonian parameters which may reflect either octahedra or next-nearest neighbour (Rb^+ and K^+ here) lattice distortions.

In order to confirm our assumptions, we undertook to determine the spin Hamiltonian parameters corresponding to the different local crystal fields in the tetragonal and in the low-temperature phases successively. This work was achieved by computing the EPR spectra.

First of all, we wrote the spin Hamiltonian related to a Gd^{3+}–O^{2-} pair:

$$\mathcal{H} = \mathcal{H}_0 + \tfrac{1}{3}b_2^0 O_2^0$$

where $\mathcal{H}_0$ stands for the Zeeman term. The less important terms of higher orders in the crystal field interaction were considered to be negligible. This expression is valid in a set of axes $OXYZ$ with $OZ \| Gd^{3+}$–O^{2-} bond and OX and OY lying along Gd–F bonds perpendicular to OZ. It remains unchanged as long as the crystal field is not modified at the Gd^{3+} site i.e. below T_{c1} in the case of rotated rigid octahedra and non-contributing next-nearest neighbours.

In the cubic phase, these $OXYZ$ sets of axes coincide with the $Oxyz$ axes directed along the fourfold cubic axes. We decided to express the spin Hamiltonians of the pairs in these fixed axes both in the tetragonal and in the low-temperature phases. Hence, the corresponding parameters were refined by adjusting the reconstructed spectra to the experimental ones.

In order to test the validity of the method, we began to simulate the EPR spectra in the tetragonal phase.

5.2.1. Reconstructed spectra in the tetragonal phase. According to Rudowicz [19], one can express the Stevens operators from an old reference frame ($OX_1Y_1Z_1$) in a new one ($OX_2Y_2Z_2$) by using a transformation matrix $\mathbf{S}(\Phi, \Theta)$ where Φ is the first rotation angle around OZ_1 and Θ is the second rotation angle around OY_2. Thus, we may write

$$\{O_n^m\} = \mathbf{S}(\Phi, \Theta)[O_n^m]$$

where the curly brackets are related to the old reference frame and the square brackets to the new one.

This leads to

$$\sum_{n,m}\{b_n^m\}\{O_n^m\} = \sum_{n,m}[b_n^m][O_n^m].$$

The $\mathbf{S}(\Phi, \Theta)$ matrices are tabulated in [19].

In the tetragonal phase, the octahedra are rotated around one of the three fourfold axes by an angle ϕ. For instance, we give in figure 7 the two reference frames in the cubic phase

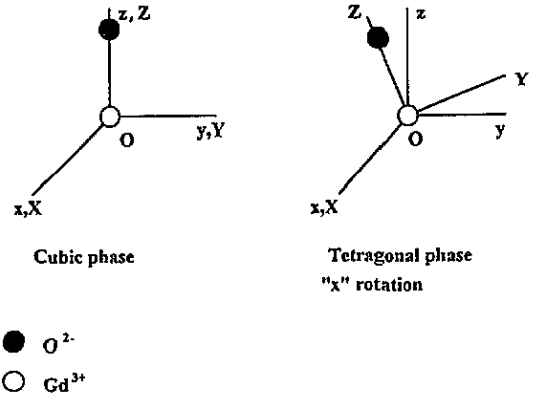

Figure 7. $OXYZ$ and $Oxyz$ in the cubic and tetragonal phases.

and in the tetragonal phase when the octahedron is rotated around the 'x' axis. So, the b_2^m parameters in the $(Oxyz)$ axis system are calculated from the $b_2^0 = -2590 \times 10^4$ cm^{-1} [15] parameter of the Gd^{3+}–O^{2-} pair in the cubic phase by considering one rotation around the x cubic axis with $\phi > 0$:

$$b_2^2 = -\tfrac{3}{2}\sin^2\phi\{b_2^0\} \qquad b_2^{-1} = -3\sin 2\phi\{b_2^0\} \qquad b_2^{0'} = \tfrac{1}{2}(3\cos^2\phi - 1)\{b_2^0\}.$$

The following points may be noted.

(i) If $\phi < 0$, only the sign of b_2^{-1} changes.

(ii) The variations of b_2^{-1} are linear with ϕ. Hence, this parameter is directly connected with the splitting of the $\pm\phi$ lines.

(iii) b_2^2 is proportional to ϕ^2 in the studied angle range.

The best result in the tetragonal phase has been obtained with experimental spin Hamiltonian parameters nearly the same as the calculated ones as given in table 2. The main difference concerns the $b_2^{\pm 2}$ values, which have to be systematically reduced to adjust the experimental spectra. Nevertheless, the signs of the calculated parameters are the correct ones.

Table 2. Calculated and experimental spin Hamiltonian parameters (in 10^{-4} cm^{-1}) in the tetragonal phase with $\phi = 4.8°$ ($T = 165$ K) ($\phi > 0$).

	b_2^{-1}		b_2^0		b_2^1		b_2^2	
	Calculated	Experimental	Calculated	Experimental	Calculated	Experimental	Calculated	Experimental
x	+1296	+1300 ±100	−2563	−2563 ±100	0	0	+27	+15 ±5
y	0	0	−2563	−2563 ±100	−1296	−1300 ±100	−27	−15 ±5
z	0	0	−2590	−2590 ±100	0	0	0	0

5.2.2. Reconstructed spectra in the low-temperature phase. With the assumptions previously described, the spin Hamiltonian parameters b_2^m were computed from the b_2^0 value of the cubic phase by considering three equal rotations around the x, y and z cubic axes in order to simulate the low-temperature phase spectra. For one Gd^{3+}–O^{2-} pair, we had to take into account 48 sets of parameters. As an example, we give in table 3 the values of the parameters at $T = 50$ K where $\phi_{[001]} = 4°$ for an 'xyz' type of rotation with $\phi_x = \phi_y = \phi_z > 0$.

Table 3. Calculated and experimental spin Hamiltonian parameters (in 10^{-4} cm^{-1}) for an '$x^+y^+z^+$' type rotation, $T = 50$ K, $\phi_{[001]} = 4°$.

$x^+, y^+, z^+,$	b_2^{-2}	b_2^{-1}	b_2^0	b_2^1	b_2^2
Calculated	+37	+1001	−2552	−1149	−5
Experimental	+90	+1001	−2552	−1150	−40
	±10	±100	±100	±100	±10

Once more, the values of the $b_2^{\pm 2}$ parameters had to be modified to adjust the experimental spectra correctly, whatever the orientation and the intensity of the static magnetic field are. The calculated and experimental values of the $b_2^{\pm 2}$ parameters for all types of rotation with positive angles are given in table 4. The experimental and reconstructed spectra of the A line when $H \| [110]$ are given as an example in figure 8. As may be seen in figure 8(b), all the components of the high-field A line are quite well reconstructed as is the splitting of the low-field line. Each component may be attributed to one Gd^{3+}–O^{2-} pair in one type of rotated octahedron.

Table 4. Calculated and experimental parameters $b_2^{\pm 2}$ (in 10^{-4} cm^{-1}), $T = 50$ K, $\phi_{[001]} = 4°$.

	b_2^{-2}		b_2^2	
	Calculated	Experimental	Calculated	Experimental
xyz yxz	±37	±90	±5	±40
xzy yzx	±40	±90	±2	±40
zxy zyx	±38	±90	0	0

From these simulations, we may conclude that all the low-temperature phase spectra in either the K or the X band, are precisely reconstructed by taking into account three rotations with equal angles. By using the same method, we have verified that the influence of the b_4^m terms is insignificant with respect to b_2^m terms.

For the highly doped crystal ($x = 0.2$), the same work was successfully achieved in spite of important linewidths with the same assumptions.

The computed simulation of the spectra was essential to support our assumptions quantitatively. Furthermore, from the spectra, we deduced the angle that may be attributed to the $\phi_{[001]}$ component of a vector $\vec{\phi}$, which would lie along the ⟨111⟩ directions.

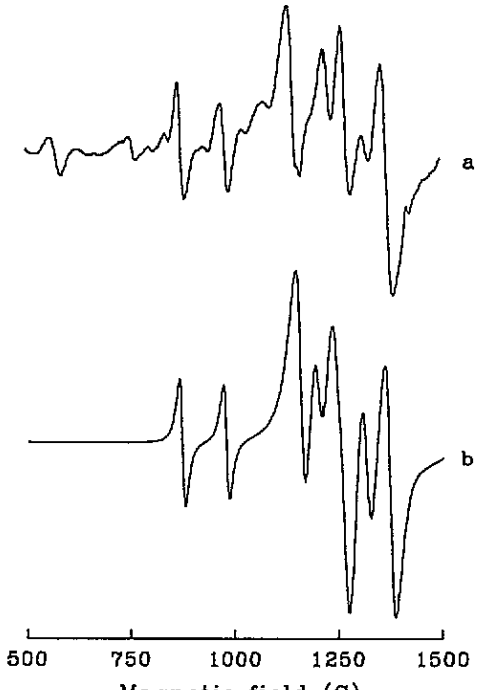

Figure 8. Experimental (*a*) and calculated (*b*) spectra in the low-temperature phase of $Rb_{0.95}K_{0.05}CaF_3$: Gd^{3+}–O^{2-} (H_{rf}‖[001], H‖[110]) ($T = 50$ K) (X band).

6. Discussion

6.1. Spin Hamiltonian parameters

In order to obtain a satisfactory agreement between experimental and simulated spectra, we had to modify b_2^m values from those deduced according to Rudowicz. These discrepancies reflect some modifications of the crystal field at the Gd^{3+} sites.

The fact that the two sets of $b_2^{\pm 1}$ values are identical proves that the Gd^{3+}–O^{2-} pair rotations reflect closely the octahedron displacements that occur at the two phase transitions. On the other hand, differences between the $b_2^{\pm 2}$ parameters occur, which may be attributed either to angular deformation of the octahedra in the plane perpendicular to Oz or to an axial contribution to the crystal field along Ox or Oy.

By using the superposition model of Newman, no angular distortions of the octahedra may be evaluated correctly in the two low-temperature phases. This leads to the conclusion that the octahedra in mixed perovskite crystals are rigid entities.

As a matter of fact, these discrepancies in the $b_2^{\pm 2}$ values may be related to distortions due to the next-nearest neighbours. In the tetragonal phase, the absolute values of these parameters are systematically smaller than the calculated ones. In perovskite type crystal, x-ray scattering measurements evidence an increase of the tetragonal cell parameter c when a decreases. This kind of distortion of the lattice cell parameters is connected to a spin Hamiltonian parameter $b_2^0 > 0$ along the c axis, which leads to contributions of the b_2^2 parameter in the pair axis system consistent with the experimental values, i.e. < 0 if c is directed along an 'x' axis and > 0 if c is along a 'y' axis. In contrast, in the low-temperature phase, the experimental spin Hamiltonian parameters $b_2^{\pm 2}$ are always larger than the calculated ones, which proves that the distortions in that phase compensate the distortions of the tetragonal phase.

6.2. Influence of the substitution on the total rotational vector of the octahedra

In the tetragonal phase, we have

$$\phi_{[001]} = \phi$$

since the octahedra are rotated around ⟨100⟩ directions.

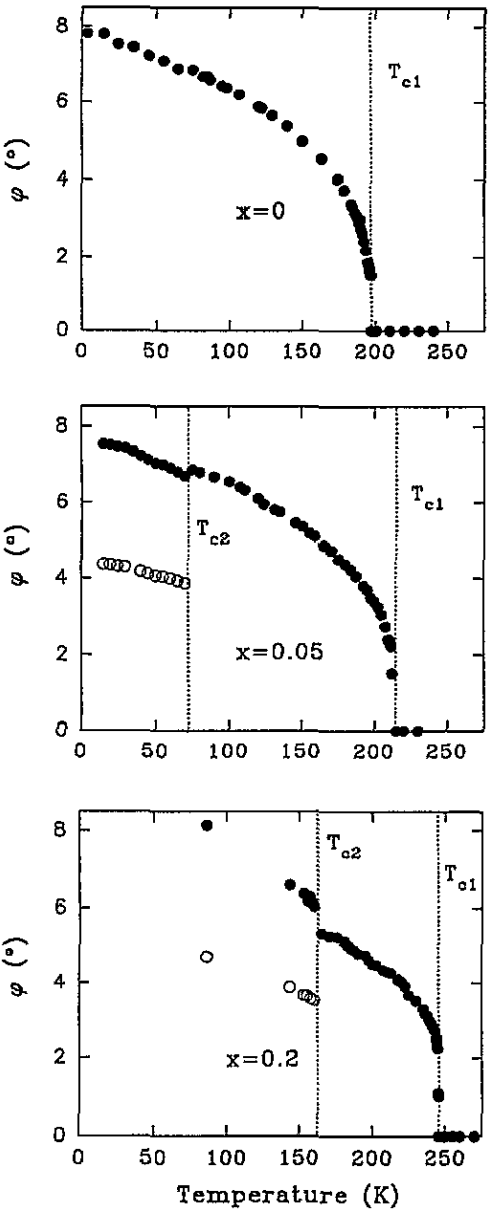

Figure 9. $\phi(T)$ as deduced from EPR measurements in $Rb_{1-x}K_xCaF_3$: Gd^{3+}–O^{2-} ($\Delta\phi = \pm 0.1°$) for $x = 0$, $x = 0.05$ and $x = 0.2$.

From figure 9, we easily see that the transition remains first order whatever the value of x is. We may notice that $\phi(T_{c1})$ decreases with the K^+ concentration.

The substitution does not affect the variations of ϕ. However, the upward shift of T_{c2} leads to a decrease of $\phi_{max} = \phi(T_{c2} + \epsilon)$ in the tetragonal phase. The tetragonality at T_{c2}

becomes less pronounced when x is increased. In the low-temperature phase, ϕ is deduced from

$$\phi = \sqrt{3}\phi_{[001]}$$

since the octahedra rotate around the three $\langle 100 \rangle$ axes with equal angles. This means that $\vec{\phi}$ may be related to a rotational vector that lies along a threefold axis. From figure 8, it may be seen that for $x = 0.05$, the variations of ϕ are only slightly affected by the substitution, while for $x = 0.2$, a discontinuity of ϕ occurs at T_{c2}. This indicates that the octahedron rotations are made easier by substituting K^+ ions with a smaller ionic radius, and corroborates the third assumption previously described in this paper.

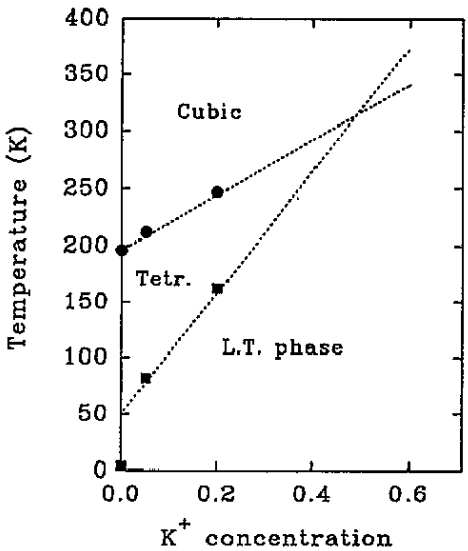

Figure 10. The phase diagram as deduced from EPR measurements in $Rb_{0.95}K_{0.05}CaF_3$: Gd^{3+}–O^{2-} at low x ($\Delta T_c = \pm 0.5$ K).

6.3. Transition temperature measurements

Accurate measurements of the transition temperatures were achieved with the K-band spectrometer from the temperature dependence of the EPR spectra obtained with $\boldsymbol{H} \| [110]$ for the two concentrations. These measurements are given in table 1. From the measurements, the phase diagram and its boundaries drawn in figure 10 evidence that the transition temperatures are enhanced and the temperature range over which the tetragonal phase occurs is strongly reduced when x increases. It is worth noting that the T_{c2} transition is more sensitive to the K^+ concentration than the T_{c1} transition:

$$dT_{c1}/dx = 2.31 \text{ K/at.\%}.$$

$$dT_{c2}/dx = 5.40 \text{ K/at.\%}.$$

The boundary line that separates the tetragonal and low-temperature phases intersects the T_c for $T_{c2} = 50$ K. This is consistent with the value deduced from neutron scattering measurements [13].

In the pure $RbCaF_3$ compound, the cubic to tetragonal transition deals with alternate octahedron rotations around the '*c*' axis, corresponding to a softening of mode at the R_{25}^{z} point of the cubic Brillouin zone. In contrast in $RbCaF_3$, the low-temperature transition is related to a simultaneous condensation of modes at the R_{25}^{x} and M_3^{y} points of the cubic Brillouin zone. According to figure 10, a crossover between the two types of transition may occur for $x = 0.5$ at $T_{c1} = T_{c2} = 310$ K. The reduction of the tetragonal distortion near T_{c2} may be connected to this competition between the two points.

The experiments under [110] uniaxial stresses have evidenced an upwards shift of T_{c1} nearly twice as large as in the pure $RbCaF_3$ when T_{c2} remains unaffected. The former result is in agreement with a more unstable cubic phase due to the substitution. The latter shows that the low-temperature phase is the stable one. Furthermore, the above-mentioned crossover should be pushed towards higher values of T_c and x under uniaxial stress.

6.4. Stability and compactness of the perovskite structure

Our results evidence that the compactness of the unit cell is directly related to the SPTs as clearly shown by Kassan-Ogly and Naish [20].

To study the AMF_3 compound stability, Goldsmidt defined a t factor as

$$t = (r_A + r_F)/\sqrt{2}(r_M + r_F)$$

where r_A, r_M and r_F are the ionic radii of the A, M and F ions respectively. The further away from unity the t factor is, the more unstable the perovskite.

It has been noticed [21] that the first transition occurs at the R point if t is close to but less than one ($SrTiO_3$, $KMnF_3$, $RbCaF_3$) while a small t factor results in a first transition associated with a soft mode at the M point of the Brillouin zone ($CsPbCl_2$). Inelastic neutron scattering studies in these compounds show that the R–M line is nearly flat: this means that alternate or non-alternate octahedron rotations are equally probable. Cowley [22] and Rousseau [23] showed that this particular behaviour is due to a competition between long- and short-range interactions. Then, it is easy to understand that the behaviour of the pure compound may be drastically modified by introducing impurities since phonon frequencies directly depend on force constants and distances between ions.

To conclude, we would like to compare our results with measurements achieved in other mixed perovskite crystals of the same type as $Rb_{1-x}K_xCaF_3$: $Rb_{1-x}K_xCdF_3$ [4], $K_{1-x}Rb_xMnF_3$ [3], $K_{1-x}Na_xMnF_3$ and $K_{1-x}Li_xMnF_3$ [5]. We considered the cubic to tetragonal SPT only.

Table 5. dT_{c1}/dx (K/at.%) for different mixed perovskite crystals.

	dT_{c1}/dx (K/at.%)
$Rb_{1-x}K_xCaF_3$	2.30
$K_{1-x}Li_xMnF_3$	10.00
$K_{1-x}Na_xMnF_3$	7.00
$Rb_{1-x}K_xCdF_3$	2.88
$Rb_xK_{1-x}MnF_3$	−3.60

From calculated dT_{c1}/dx values (table 5), we may infer that the more stable the pure perovskite is, the more sensitive it is to the substitution. The variations of T_{c1} versus $1 - t$, which are characteristic of the discrepancy from the ideal perovskite, are shown in figure 11. The t factors were calculated from ionic radii given in [24], and we consider that F^- is twofold coordinated in the M–F bond and fourfold coordinated in the A–F bond. This graph shows two important features:

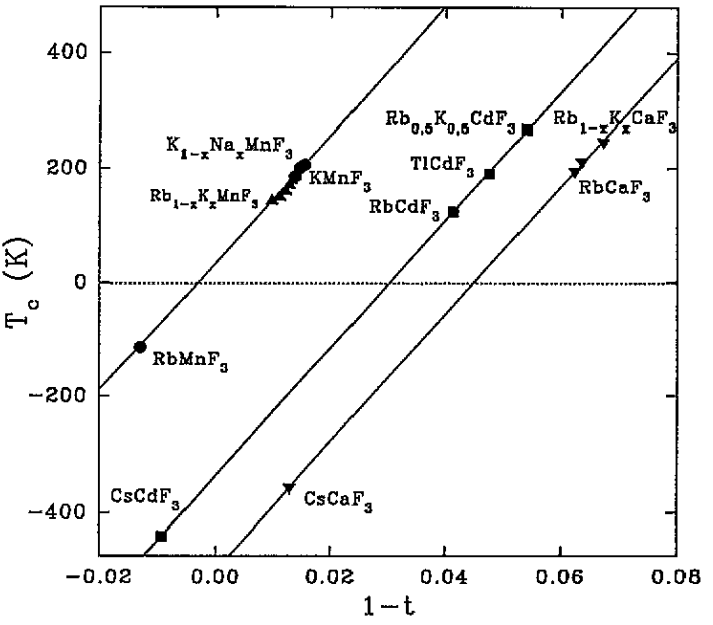

Figure 11. T_{c1} versus $1-t$ deduced from experimental measurements in mixed crystals.

(i) $Rb_{1-x}K_xCaF_3$ is the less stable perovskite and

(ii) $1-t$ increases when the substituted ion is bigger than the substitutional one. This leads to an increase of the transition temperature.

We calculated $dT_{c1}/d(1-t)$ for all these compounds except $K_{1-x}Li_xMnF_3$, for which no value of Li^+ ionic radius is given in [24]. Furthermore, the substitution may take place at the octahedron centre as in $BaLiF_3$. From these calculations, we deduce that T_{c1} varies linearly versus $1-t$:

$$T_{c1}(1-t) = A(1-t) + T_c(0)$$

where

$$A = (1.1 \pm 0.1) \times 10^4 \text{ K}$$

$T_{c1}(0) = 35$ K for $K_{1-x}Na_xMnF_3$ and $Rb_{1-x}K_xMnF_3$

$T_{c1}(0) = -337$ K for $K_{1-x}Na_xMnF_3$

$T_{c1}(0) = -501$ K for $K_{1-x}Na_xMnF_3$.

Owing to the corresponding $1-t$ values, the transition temperatures deduced from this diagram are negative for the three perovskites $RbMnF_3$, $CsCaF_3$ and $CsCdF_3$. No transition should be observed, in agreement with experimental observations.

It seems important to notice the following from this diagram.

(i) $1-t$ is characteristic of the structural instability. The main parameter of the problem is t rather than the substitutional ratio x.

(ii) $dT_{c1}/d(1-t)$ depends directly on the type of substitution but is constant for each type of substitution. It would be worth trying some new experiments on compounds such as $RbCa_{1-x}Zn_xF_3$ and $KCa_{1-x}Zn_xF_3$.

All these results may be quite easily understood if we keep in mind that the substitution of Rb^+ by K^+ with smaller ionic radius reduces the compactness of the cell and destabilizes the cubic structure.

References

[1] Buzaré J Y and Foucher P H 1991 *J. Phys.: Condens. Matter* **3** 2535
[2] Minorel A M, Silly G and Buzaré J Y 1991 *Ferroelectrics* **124** 297
[3] Borsa F, Bernard D J, Walker W C and Baviera A 1977 *Phys. Rev.* B **15** 84
[4] Hidaka M, Zhou Z Y and Yamashita S 1990 *Phase Trans.* **20** 83
[5] Ratuszna A 1993 *J. Phys.: Condens Matter* **5** 841
[6] Berlinger W and Müller K A 1977 *Rev. Sci. Instrum.* **48** 1161
[7] Berlinger W 1982 *Rev. Sci. Instrum.* **53** 338
[8] Berlinger W 1985 *Magn. Res. Rev.* **10** 45
[9] Buzaré J Y, Rousseau J J and Fayet J C 1977 *J. Physique Lett.* **38** L445
[10] Müller K A 1976 *Proc. Int. School Phys. 'Enrico Fermi'* Course LIX (Amsterdam: North Holland)
[11] Buzaré J Y, Fayet-Bonnel M and Fayet J C 1981 *J. Phys. C: Solid State Phys.* **14** 67
[12] Simon P, Rousseau J J and Buzaré J Y 1982 *J. Phys. C: Solid State Phys.* **15** 5741
[13] Bulou A, Ridou C, Rousseau M, Nouet J and Hewat A W 1980 *J. Physique* **41** 87
[14] Ridou C, Rousseau M and Bouillot J 1981 *Ferroelectrics* **36** 463
[15] Buzaré J Y, Fayet J C, Berlinger W and Müller K A 1979 *Phys. Rev. Lett.* **42** 465
[16] Buzaré J Y, Berlinger W and Müller K A 1985 *J. Physique. Lett.* **46** L201
[17] Buzaré J Y, Berlinger W and Müller K A 1989 *Europhys. Lett.* **10** 739
[18] Buzaré J Y, Berlinger W and Müller K A 1991 *Ferroelectrics* **124** 303
[19] Rudowicz C 1985 *J. Phys. C: Solid State Phys.* **18** 1415
[20] Kassan-Ogly F A and Naish V E 1986 *Acta Crystallogr.* B **42** 325
[21] Gibaud A, Shapiro S M, Nouet J and You H 1991 *Phys. Rev.* B **44** 2437
[22] Cowley R A 1964 *Phys. Rev.* **134** 981
[23] Rousseau M, Nouet J and Almairac R 1977 *J. Physique* **38** 1423
[24] Shannon R D 1976 *Acta Crystallogr.* A **32** 751